ORIGINAL PAPER

Facile room-temperature synthesis of cetyltrimethylammonium bromide (CTAB) coated spherical silver nanoparticles and their surface-enhanced Raman scattering (SERS) and antibacterial applications

Hania Feroz Mughal[1] · Ghazanfar Ali Khan[1] · Muhammad Shafiq[2] · Muhammad Zeeshan Hyder[2] · Waqqar Ahmed[1]

Abstract

Silver nanoparticles (AgNPs) are appealing due to their cost-effectiveness and remarkable capabilities in sensing and antibacterial applications. Herein, we report a facile near room-temperature synthesis of AgNPs capped with a cationic surfactant using a single-step recipe. The AgNPs were synthesized by reducing silver ions with ascorbic acid in a basic reaction medium, and in the presence of cetyltrimethylammonium bromide (CTAB). By varying the concentration of CTAB and the pH of the reaction medium, the yield of the AgNPs can be tuned. The essential experimental conditions supporting the high yield of uniform AgNPs are 10 mM concentration of CTAB and a strong basic pH. The impact of aging on AgNPs was also investigated by examining changes in their ultraviolet–visible (UV–Vis) spectra over time. The AgNPs, purified by centrifugation and redispersed in CTAB solution, showed reliable shelf-life under both light and dark storage conditions. Furthermore, the synthesized AgNPs showed excellent surface-enhanced Raman scattering (SERS)-based trace detection toward anionic dye, methyl orange (MO). The AgNPs allowed detecting MO down to 10^{-10} M. Finally, the AgNPs also exhibited good antibacterial activity against two gram-positive bacteria, namely *Enterococcus* spps. and *Staphylococcus aureus*.

Keywords Silver nanoparticles · Cetyltrimethylammonium bromide (CTAB) · Surface-enhanced Raman scattering (SERS) · Antibacterial · Methyl orange · *Enterococcus* spps. · *Staphylococcus aureus*

Introduction

Noble metal nanoparticles (NPs) have attracted great attention since they offer unique properties that can be tailor-made for specific applications including SERS and antibacterial activity (Jiang et al. 2005; Saini et al. 2010; Pathakoti et al. 2017; Venditti et al. 2017; Zia et al. 2018). The electromagnetic waves can generate zones of enhanced electric fields on the surface of metallic NPs under resonance conditions due to the surface plasmon resonance (SPR). The SPR is very sensitive to the composition, size, shape, and interparticle spacing of the NPs (Busbee et al. 2003). Among various plasmonically active NPs, the most well-recognized are Ag and Au (Steinbrück et al. 2009; Youssef et al. 2014). Silver NPs are interesting due to their low-cost and excellent SERS and antibacterial properties. The plasmonic properties of Ag are superior to that of Au due to minimal damping (Mayer et al. 2017), which makes Ag the most active material for fabricating sensitive and cost-effective SERS sensors.

There is historical evidence of the use of Ag for antibacterial purposes dating back to ancient Rome (Medici et al. 2019). However, the scientific exploration of the mechanisms of the antibacterial action of the AgNPs has only gained pace recently (Medici et al. 2019). Their antimicrobial applications increased greatly after Ivan Sondi and colleagues put forward a comprehensive work in 2004 demonstrating AgNPs as a new type of bactericidal material (Sondi and Salopek-Sondi 2004). Silver NPs are active against the broad spectrum of bacteria and effective in inhibiting bacterial growth (Inoue et al. 2002). More significantly,

✉ Waqqar Ahmed
  w.ahmed@comsats.edu.pk

[1] Materials Laboratory, Department of Physics, COMSATS University Islamabad, Park Road, Islamabad 45500, Pakistan

[2] Department of Biosciences, COMSATS University Islamabad, Park Road, Islamabad 45500, Pakistan

AgNPs provide a viable alternate to antibiotics, presenting a potential solution to the issue of bacterial multidrug resistance (Franci et al. 2015).

The antibacterial activity of AgNPs is sensitively dependent on their size, shape, and surface charge (El Badawy et al. 2011; Sohm et al. 2015; Slavin et al. 2017; Tang and Zheng 2018). The positively charged AgNPs are more effective than their negatively charged counterparts for antibacterial activities. This is because the cell walls of both gram-positive and gram-negative bacteria have a net negative surface charge, which enables the positively charged NPs to effectively bind to their surface (Abbaszadegan et al. 2015). The antibacterial action of AgNPs is especially significant for gram-positive bacteria as they have thick outer layer and are generally difficult to sterilize. Therefore, it is important to develop positively charged AgNPs which are active against gram-positive bacteria.

One of the limitations of AgNPs is that they are prone to oxidation. The oxidation process of AgNPs intensifies when they are exposed to light (Mahapatra and Karak 2008; Li et al. 2013). The formation of the Ag oxide (Ag_2O) layer is energetically favorable at room temperature and is even observed in the presence of organic surfactants (Hiramatsu and Osterloh 2004; Jiang et al. 2006). Therefore, synthesizing AgNPs which are less susceptible to oxidation is crucial for preserving their inherent properties and their practical applicability.

Silver NPs can be synthesized using diverse physical and chemical methods (Iravani et al. 2014). Many physical synthesis methods, including physical vapor deposition, arc-discharge, and laser ablation demand sophisticated equipment, consume higher energy, require substantial space, and necessitate regular maintenance. Consequently, these approaches tend to be more costly (Magnusson et al. 1999; Kruis et al. 2000; Mafuné et al. 2000; Darroudi et al. 2011). On the other hand, chemical methods used for the synthesis of AgNPs are comparatively straightforward, allowing for easy tuning of NP size and shape by adjusting the concentrations of a few key reagents [27]. However, some of these methods require rigorous synthesis and/or high temperatures. For example, high-temperature synthesis of AgNPs has been reported using ethylene glycol as a reducing agent in the presence of polyvinylpyrrolidone (PVP). Few of the citrate-based methods also require the use of high reaction temperatures for the effective synthesis of AgNPs (Sun et al. 2002). For instance, the Lee–Meisel method involves the reduction of silver nitrate ($AgNO_3$) with sodium citrate at temperatures approaching 100 °C. Additionally, the anionic nature of citrate-capped nanoparticles poses limitations in SERS-based trace detection of anionic analytes, as it leads to electrostatic repulsions. Similarly, this characteristic can limit their effectiveness in antibacterial applications (Si et al. 2009). Environmentally friendly biological methods could require high temperatures, e.g., the synthesis of AgNPs using pomegranate shells require 300 °C (Gamboa et al. 2019).

A cationic surfactant CTAB has also been employed for the synthesis of AgNPs of various shapes (Jana et al. 2001a; Murphy et al. 2005). Usually, a seed-mediated method is followed, which involves the synthesis of a few nanometers of Ag seed particles and their subsequent addition to a growth solution. The growth solution generally consists of Ag precursor, CTAB, and a reducing agent, ascorbic acid. Ascorbic acid is a weak reducing agent that cannot reduce Ag ions in a solution containing a high concentration of CTAB (Jana et al. 2001b; Abdullah et al. 2018). When the seed particles are added to the solution, they provide a catalytic effect, which helps the reduction of Ag ions on top of the seeds (Slavin et al. 2017). This way seeds grow into NPs. Although this method is effective, it involves multiple steps, which complicates the synthesis. Recipes involving high temperatures or multiple steps are also difficult to scale up, especially for the reactor-based continuous flow synthesis (Liu et al. 2013). Therefore, a facile, single-step, near-room temperature, synthesis of positively charged, and stable AgNPs is still needed.

In this study, we have synthesized AgNPs coated with CTAB with a near-room-temperature single-step method. Through systematic variations in the concentrations of CTAB and NaOH, we demonstrate precise control over the yield of AgNPs. The synthesized AgNPs are further employed for the SERS and antibacterial applications. Specifically, these AgNPs exhibit exceptional trace detection sensitivity toward MO and also displayed significant antibacterial activity against gram-positive bacteria, Enterococcus species and Staphylococcus aureus.

Experimental

Materials

All the chemicals, i.e., $AgNO_3$ (ChemLab, 99.9%), CTAB (Sigma, ≥ 99%), ascorbic acid (Sigma, 99%), NaOH (Sigma, 99%), MO (Sigma, 99%) were used without further purification and their solutions were prepared using de-ionized (DI) water as solvent.
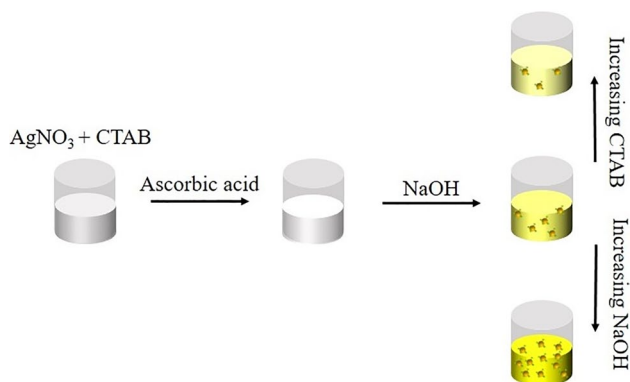
Synthesis of AgNPs

Silver NPs were synthesized via a single-step method. In a typical synthesis, $AgNO_3$ (50 μL, 0.1 M) was added to 10 ml of CTAB solution of molarities ranging from 0.01 to 0.2 M. To this solution, 60 μL of 0.1 M ascorbic acid was added, which was followed by the addition of 600 μL of 0.2 M NaOH under continuous stirring. Afterward, the solution was left undisturbed for 2 h at about 25 °C.

As soon as NaOH was added to the precursor solution, the color of the solution gradually changed from transparent to pale yellow and finally to greenish indicating the formation of AgNPs. The samples were left undisturbed overnight. The concentration of NaOH (0.2 M) was also systematically varied, ranging from 100 to 500 μl in increments of 100 μl, to see the effect of the solution's pH on the synthesis. The schematic of growth is shown in Fig. 1.

Finally, 1 mL of the colloidal suspension was added to 6 Eppendorf tubes each, and centrifuged twice at 10,000 rpm for 10 min. The precipitates settled at the bottom; while, the supernatant containing excess reactants and byproducts was carefully removed using a micropipette. The precipitates were redispersed in equal volume of DI water after the initial centrifugation step. Following the second centrifugation step, the precipitates were redispersed in varying volumes of DI water (1 mL, 500 μL, 200 μL, 100 μL, 50 μL, and 20 μL), yielding AgNPs suspensions of different concentrations, labeled as $1\times$, $2\times$, $5\times$, $10\times$, $20\times$ and $50\times$, respectively. The $1\times$ suspension of AgNPs corresponds to a concentration of 0.054 mg/mL.

Characterization

The absorption properties and morphology of AgNPs were characterized using UV–Vis spectroscopy and transmission electron microscopy (TEM). The UV–Vis absorption measurements were taken using a UV-1280 Shimadzu Spectrophotometer operating over the wavelength range of 300–800 nm. The TEM analysis was done using FEI Tecnai G2 Spirit Biotwin TEM. The CTAB coating was verified by measuring the Zeta potential of the solution using Malvern Zetasizer and Fourier Transform Infrared Spectroscopy (FTIR) analysis using a Thermo Scientific Nicolet iS10 spectrometer.

Fig. 1 Schematics of AgNPs synthesis

Aging experiments

For the aging experiments, AgNPs synthesized with 0.025 M CTAB were used. The samples were aged both in light and dark storage conditions. Silver NPs were aged in three distinct colloidal environments to evaluate their stability. First, the particles were centrifuged and redispersed in equal volume of DI water. The samples aged in light and dark were labeled as DI-light and DI-dark, respectively. Second, the centrifuged particles were redispersed in equal volume of 1 mM CTAB solution. The samples aged in light and dark, in this case, were labeled as CTAB-light and CTAB-dark, respectively. Third, the as-prepared AgNPs were left in the growth solution. The samples aged in light and dark were labeled as AP-light and AP-dark, respectively. The UV–Vis spectra were collected at different intervals over two months to examine if there was any change in the particle composition or morphology.

SERS analysis

The SERS measurements were taken using a Dongwoo Optron Raman system equipped with a 514 nm laser excitation source. A laser power of 5 mW, an exposure time of 10 s, and a $100\times$ objective lens were employed to capture the Raman spectra. A 10 μL droplet of purified AgNPs suspension ($20\times$ concentration) was dried on Si substrates. Subsequently, a 10 μL droplet of MO solution of varying concentrations, i.e., 10^{-6}–10^{-11} M was dried on the substrates and the Raman spectra was taken. To obtain the blank spectrum, the Raman spectrum of AgNPs without MO was taken.

Antibacterial activity test

The antibacterial activity of AgNPs was tested using the agar well diffusion method (du Toit and Rautenbach 2000), against two gram-positive bacteria, *Enterococcus* spps. and *Staphylococcus aureus*. A lawn of bacteria having 1.5×10^8 CFU/mL density was made on Mueller Hinton agar (MHA containing petri plates). Small wells were made using a sterile borer. Concentrations of AgNPs at $1\times$, $2\times$, $5\times$, and $10\times$ were used against *Enterococcus* spps.; while, concentrations of $2\times$, $10\times$, and $50\times$ were utilized against *Staphylococcus aureus*. A 10 μL volume of each concentration of AgNPs was added to these wells. Therefore, the added mass of AgNPs were 0.54 μg, 1.08 μg, 2.7 μg and 5.4 μg, for *Enterococcus* spps., and 1.08 μg, 5.4 μg and 27 μg for *Staphylococcus aureus*. These plates were then placed in an incubator for 24 h and their zones of inhibition (ZOI) were measured with the help of a calibrated scale.

Results and discussion

The UV–Vis spectroscopy was carried out to confirm the formation of AgNPs. Initially, the effect of different concentrations of CTAB was tested keeping all other reaction parameters the same. The CTAB concentration was varied from 0.01 to 0.2 M, as shown in Fig. 2a. Although there is no radical change in the plasmon peak position, there is a clear progressive decrease in the intensity of the plasmon peak with increasing CTAB concentration. For 0.01 M CTAB concentration, the UV–Vis absorption peak has an intensity of 1.5 which decreases to 0.019 for 0.2 M CTAB concentration. This represents a decrease in particle

concentration with increasing CTAB concentration. At CTAB concentrations below 0.01 M, partial aggregation of AgNPs occurred during the purification steps. When the CTAB concentration was 0.5 mM or lower, a noticeable change in the solution's color appeared upon the addition of ascorbic acid (prior to NaOH addition), signaling the formation of AgNPs. However, these NPs tend to aggregate during overnight aging.

The growth evolutions of AgNPs with time were tested for varying CTAB concentrations and is shown in Fig. 2b–g. In all cases, there is an increase in the plasmon peak intensity. The plasmon peak intensity versus time for various CTAB concentrations has been plotted in Fig. 2h. As evident from the figure, there is an initial fast increase in the plasmon peak
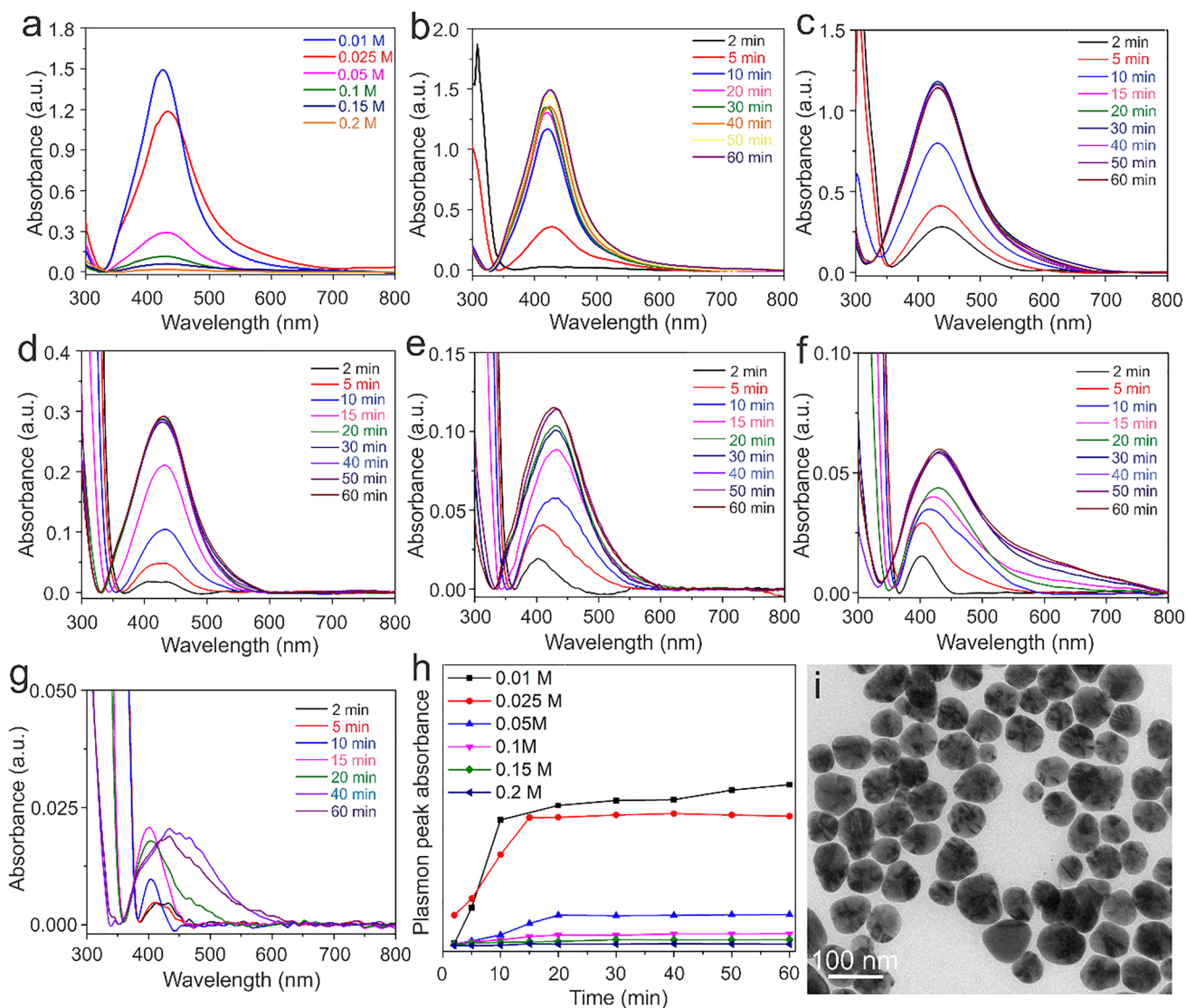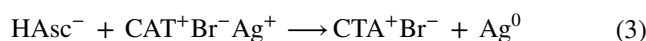

Fig. 2 UV–Vis spectra of AgNPs prepared at different CTAB concentrations (**a**); time evolution growth of AgNPs at 0.01 M (**b**), 0.025 M (**c**), 0.05 M (**d**), 0.1 M (**e**), 0.15 M (**f**), 0.2 M (**g**) CTAB; time evolu-

tion of the plasmon peak for AgNPs prepared at different CTAB concentration (**h**); TEM image of AgNPs prepared with 0.025 M CTAB (**i**)

intensity which subsequently slows down and saturates after a while. With increasing CTAB concentration, the growth is progressively slower with a lower final plasmon peak intensity. Two conclusions can be made from the growth evolution study: first, the rate of growth of NPs becomes slower with increasing CTAB concentration; second, the plasmon peak saturates at lower intensities with increasing CTAB which indicated a lower yield of AgNPs. Figure 2i shows the TEM image of AgNPs synthesized with 0.025 M CTAB. It is verified that synthesized NPs are near-spherical in shape and have an average diameter of 59 ± 16 nm.

The yield and uniformity of the synthesized AgNPs can also be modulated by adjusting the pH of the reaction medium by varying the concentration of NaOH. This is evident from Fig. 3a which depicts the UV–Vis spectra of samples prepared at different pH values. The area under the plasmon peak serves as a rough indicator of the AgNP concentration, reflecting the yield of the reaction, i.e., the conversion of Ag ions to Ag^0. As depicted in Fig. 3a, it is evident that at the lowest pH value of 10.4, the yield is significantly low. However, for samples synthesized at a pH of 11.1 and higher, the areas under the plasmon peaks are within 10% of each other, suggesting that the reaction yield remains relatively consistent even with further increases in pH. However, the broadening of the plasmon peak reduces with an increase in pH, indicating that nanoparticles synthesized at higher pH values exhibit relatively less size dispersion.

It has been reported that the addition of AgNO₃ in the CTAB solution leads to the formation of the Ag^+-CTAB complex. Li et al. (2012) used FTIR to demonstrate the complexation of Ag with CTAB. Liu et. al. carried out an XPS analysis to study the coordination of Ag with CTAB. They showed that Ag coordinated complex has a stronger Ag–Br and a weaker Ag–N coordination bond (Liu et al. 2007). Under such conditions, it is difficult to reduce Ag ions. However, an increase in the pH of the solution increases the reduction strength of ascorbic acid (H_2ASc). The first pKa of ascorbic acid is 4.1, which means that at a high pH value, ascorbic acid deprotonates into ascorbate anions $HAsc^-$. Due to its better reduction power, ascorbate can reduce Ag ions from the Ag-CTAB complex (Busbee et al. 2003). Below are the details of the reactions,

$$CTA^+Br^- + AgNO_3 \rightarrow CTA^+Br^-Ag^+ + NO_3^- \tag{1}$$

$$H_2Asc \left(\frac{NaOH}{pK_1 = 4.1} \right) \longrightarrow HAsc^- + H^+ \tag{2}$$

$$HAsc^- + CAT^+Br^-Ag^+ \longrightarrow CTA^+Br^- + Ag^0 \tag{3}$$

When the Ag^0 concentration reaches supersaturation, nucleation of Ag occurs. These Ag nuclei can grow further with the relatively easier autocatalytic reduction of Ag ions on top of them. The presence of a high concentration

Fig. 3 UV–Vis spectra of AgNPs synthesized at different pH values synthesized with 0.025 M CTAB concentration; the pH was increased by changing the added volume of 0.2 M NaOH from 100 to 500 µl in increments of 100 µl (**a**); FTIR spectrum of AgNPs (**b**); Zeta potential of AgNPs (**c**); comparison of the change in the plasmon peak position with time under different storage conditions (**d**)
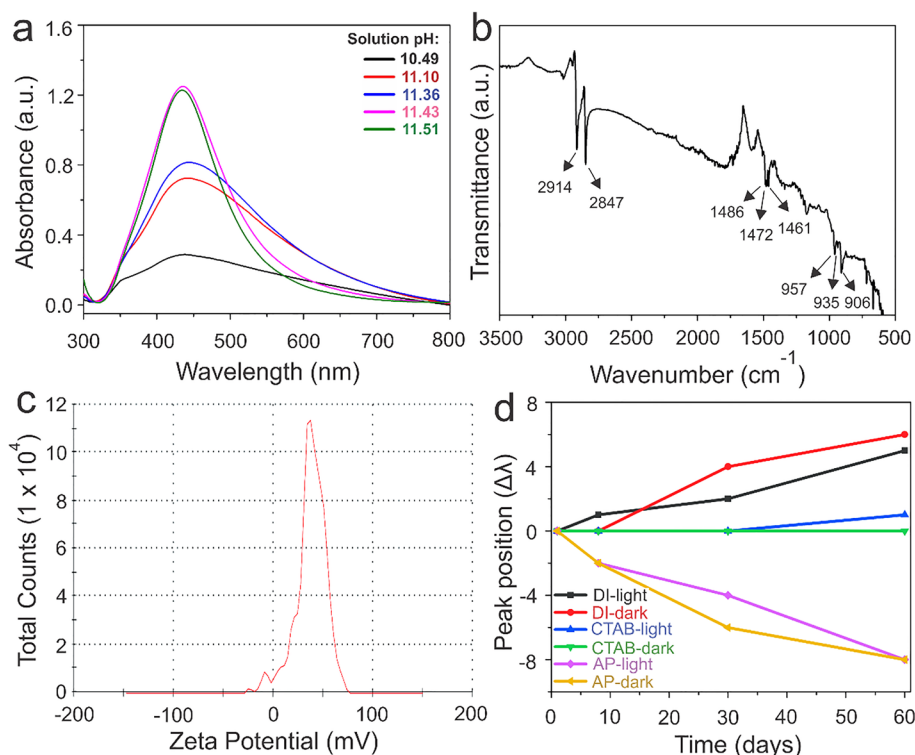
of CTAB hinders the reduction of Ag ions, and therefore, affects both nucleation and growth rates. This explains the slower growth kinetics for higher CTAB concentrations as observed in Fig. 2h. Moreover, the difficulty in reduction of Ag ions with increasing CTAB concentration also results in the lower final yield of NPs, which is also evident from the saturation of the plasmon peak at lower intensities (Fig. 2h).

On the other hand, an increase in the concentration of NaOH for a fixed CTAB concentration has been shown to increase the yield of AgNPs. This can be explained by the fact that under elevated pH reaction conditions, a high concentration of $HAsc^-$ is available, which has a better reduction capability compared to ascorbic acid, as discussed before. This results in the better reduction efficiency of Ag ions, leading to the formation of a higher concentration of AgNPs. However, for a certain concentration of NaOH in the growth solution, the reduction of Ag^+ to Ag^0 is probably complete. Therefore, no further increase in NPs production can be seen for even higher NaOH concentrations. This is exactly what we see in our experimental results (Fig. 3a).

The CTAB coating on AgNPs was confirmed by FTIR analysis. Figure 3b depicts the FTIR spectra of the AgNPs powder. The band at 2914 and 2847 cm^{-1} corresponds to the symmetric and anti-symmetric stretching of $-CH_2-$, respectively (Khan et al. 2019). The C–H scissoring vibration of N^+-CH_3 moiety is represented by the bands at 1486 cm^{-1}, 1472 cm^{-1}, and 1461 cm^{-1} (Khan et al. 2019). Therefore, the FTIR analysis verifies the coverage of AgNPs by CTAB.

To verify the surface charge of AgNPs due to the presence of CTAB on their surface, we carried out the Zeta potential analysis. As depicted in Fig. 3c, the particles have a Zeta potential value of $+37.4$ mV, which verifies the positive surface charge of AgNPs. Therefore, Zeta potential analysis, along with the FTIR analysis, verifies the CTAB coating of AgNPs.

Stability of AgNPs

Figure 3d depicts the variation of the plasmon peak position with time for the AgNPs dispersed in different mediums both in light and dark environments, as described in the experimental section. The plasmon peak position did not change much with time for the NPs dispersed in the CTAB solution. We observed no change for the solution kept in dark and a change of only 1 nm for the solution kept in the light. However, there was a red-shift in the peak for NPs dispersed in DI water. This could be due to the Ostwald ripening (Kabalnov 2001). The disintegration of smaller NPs and further growth of larger NPs may result in shifting in the plasmon peak to the longer wavelengths. Moreover, the aggregation of AgNPs may result in the formation of bigger NP clusters which may result in the red-shift of the plasmon peak. For AgNPs dispersed in 1 mM CTAB solution, the

CTAB bilayer stays stable. The CTAB bilayer on particle's surface reduces its surface energy. Therefore, the Ostwald ripening and NP aggregation is prevented for the particles dispersed in CTAB solution. However, for the AgNPs dispersed in DI water, the change could be due to the weakening of the CTAB bilayer, which could cause disintegration of relatively smaller AgNPs, or aggregation of AgNPs.

Surprisingly when the NPs were left in the growth solution, the plasmon peak blue-shifted, indicating a decrease in particle size. The reduction of particle size could be caused by the oxidative etching of the NPs and a decrease in their size. Overall we have seen the trends of change of the plasmon peak position in all cases are similar for the storage under light and dark conditions. Therefore, exposure to light does not result in producing any changes in the morphology of AgNPs. Moreover, we conclude that the AgNPs have the best shelf-life when they are purified by centrifugation and redispersed in CTAB solution.

SERS

The synthesized AgNPs were deposited on the substrate to check their SERS-based trace detection capabilities. For this purpose, we have chosen an anionic dye, MO, to benefit from the cationic nature of the surfactant CTAB. Figure 4 depicts the SERS spectra of various concentrations of MO dried on top of AgNPs, the fingerprint Raman peaks of MO appear in the spectra. The most prominent peaks were at 1129 cm^{-1}, 1157 cm^{-1}, 1466 cm^{-1}, and 1643 cm^{-1}, which agrees well with the reported literature (Jia et al. 2008; Vorob'ev et al. 2018). The peaks at 760 cm^{-1} and 1445 cm^{-1}, correspond to the Raman modes of CTAB molecules surrounding the AgNPs (Yu et al. 2007). It is evident
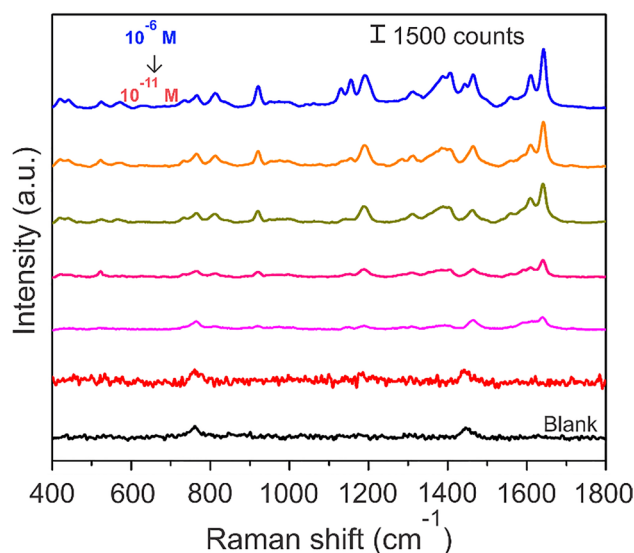

Fig. 4 SERS spectra of different concentrations of MO

from Fig. 4 that concentrations as low as 10^{-10} M were easily detected, with a good signal-to-noise ratio. However, the spectrum of 10^{-11} M MO concentration did not show any Raman modes of MO. The limit of detection (LoD) obtained in this work is lower compared to other reported results of SERS-based trace detection of MO, as shown in Table 1. The better sensitivity, in this case, could be due to the opposite polarity of CTAB-coated AgNPs and MO, which enables MO molecules to efficiently adsorb close to the surface of AgNPs. Therefore, the SERS substrates fabricated from AgNPs are excellent for SERS-based trace detection of anionic analytes.

The enhancement factor (EF) was calculated using the following equation (Abdullah et al. 2018),

$$EF = \frac{(I_{SERS} \times C_{Bulk})}{I_{Raman} \times C_{SERS}}$$

where I_{SERS} and I_{Raman} are the intensities of peaks at 1643 cm^{-1} for SERS and reference Raman measurements, respectively, and C_{SERS} and C_{Bulk} are the concentrations used for SERS and reference Raman measurements, respectively. The reference measurement was carried out using 0.01 M MO without AgNPs, while for SERS measurements 10^{-6} M MO was used. The experimental enhancement factor was calculated to be 1.28×10^6.

Antibacterial activity

Well diffusion method was used to test the antibacterial effect of AgNPs against two gram-positive bacteria,

Enterococcus spps. and *Staphylococcus aureus*. As depicted in Fig. 5a, b, there are clear ZOI around wells which increase with increasing AgNPs concentration. The ZOI expanded from a diameter of 10 to 14 mm for *Enterococcus* spps. as the concentration of AgNPs increased from 0.54 to 5.4 μg. Similarly, for *Staphylococcus aureus*, the ZOI grew from 8 to 10 mm as the AgNPs concentration changed from 1.08 to 27 μg, as illustrated in Fig. 5c.

As mentioned before, the negatively charged surface of gram-positive bacteria enhances the adhesion of positively charged AgNPs to their outer membrane, facilitating a more effective interaction. Therefore, we believe that the CTAB-capped AgNPs have a better chance of accumulating on the negatively charged cell wall, compared to the negatively charged AgNPs. This leads to increased permeability of the cell wall. The interaction of the AgNPs with the peptidoglycan changes its configuration, therefore, causing damage to the cell wall and resulting in bacterial death (Shu et al. 2020).

Conclusions

We have developed a facile and single-step recipe for the synthesis of AgNPs near room temperature. We showed that the AgNPs can be synthesized by reducing $AgNO_3$ with ascorbic acid in a growth medium containing CTAB when high pH reaction conditions are employed. The growth kinetics can be controlled by changing the CTAB concentration and pH of the reaction medium. The yield of AgNPs increases by decreasing the CTAB concentration in

Table 1 Comparison of our SERS results with previous reports

Templates	LoD	References
AgNPs and Cu$_2$O microcubes hybrid	10^{-9} M	Pham et al. (2023)
AgNPs on eggshell membranes	10^{-9} M	Candido et al. (2019)
AgNPs functionalized with mono-6-deoxy-6-thio-β-cyclodextrin	5×10^{-7} M	Liu et al. (2020)
AgNPs on single-layer porous silicon	10^{-8} M	Van Nguyen et al. (2021)
AgNPs on porous silicon photonic crystals	10^{-9} M	Van Nguyen et al. (2021)
AgNPs on Si substrate	10^{-10} M	This work

Fig. 5 Inhibition zone photographs of 0.54 μg (1), 1.08 μg (2), 2.7 μg (3), and 5.4 μg (4) of AgNPs against *Enterococcus* spps. (**a**); and 1.08 μg (1), 5.4 μg (2), and 27 μg (3) of AgNPs against *Staphylococcus aureus* (**b**). Histogram of the diameter of zone of inhibition (**c**)
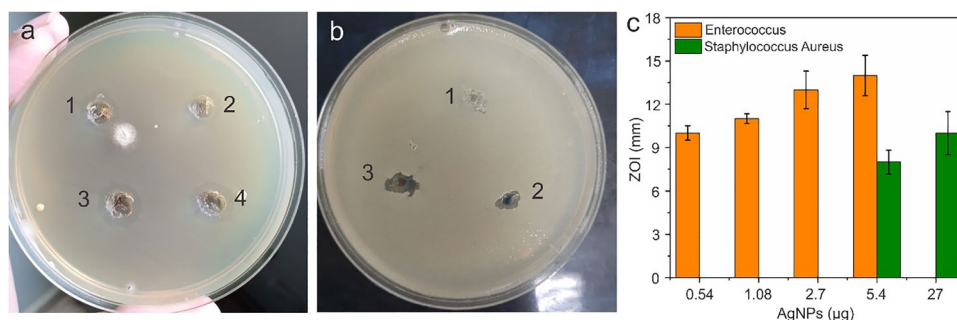
the growth solution, and also by increasing the pH of the solution. The synthesized AgNPs have excellent shelf-life, both when stored under light and in darkness, when they are suspended in CTAB solution. Owing to the positive surface charge, AgNPs have shown excellent SERS-based trace detection capabilities for the detection of anionic dye MO. The dye concentration as low as 10^{-10} M has been detected using AgNPs as SERS substrates. The positive surface charge of AgNPs also makes them promising nanomaterials against the gram-positive bacteria. The AgNPs have shown good antibacterial activity against *Enterococcus* spps. and *Staphylococcus aureus.*

Declarations

Conflict of interest All the authors declare that they have no conflict of interest.

References

Abbaszadegan A, Ghahramani Y, Gholami A et al (2015) The effect of charge at the surface of silver nanoparticles on antimicrobial activity against gram-positive and gram-negative bacteria: a preliminary study. J Nanomater 2015:1–8

Abdullah A, Altaf M, Khan HI et al (2018) Facile room temperature synthesis of multifunctional CTAB coated gold nanoparticles. Chem Phys 510:30–36

Busbee BD, Obare SO, Murphy CJ (2003) An improved synthesis of high-aspect-ratio gold nanorods. Adv Mater 15:414–416

Candido ICM, Soares JMD, de Barbosa ABJ, de Oliveira HP (2019) Adsorption and identification of traces of dyes in aqueous solutions using chemically modified eggshell membranes. Bioresour Technol Rep 7:100267

Darroudi M, Ahmad MB, Zak AK et al (2011) Fabrication and characterization of gelatin stabilized silver nanoparticles under UV-light. Int J Mol Sci 12:6346–6356

du Toit EA, Rautenbach M (2000) A sensitive standardised micro-gel well diffusion assay for the determination of antimicrobial activity. J Microbiol Methods 42:159–165

El Badawy AM, Silva RG, Morris B et al (2011) Surface charge-dependent toxicity of silver nanoparticles. Environ Sci Technol 45:283–287

Franci G, Falanga A, Galdiero S et al (2015) Silver nanoparticles as potential antibacterial agents. Molecules 20:8856–8874

Gamboa SM, Rojas ER, Martínez VV, Vega-Baudrit J (2019) Synthesis and characterization of silver nanoparticles and their application as an antibacterial agent. Int J Biosen Bioelectron 5:166–173

Hiramatsu H, Osterloh FE (2004) A Simple large-scale synthesis of nearly monodisperse gold and silver nanoparticles with adjustable sizes and with exchangeable surfactants. Chem Mater 16:2509–2511

Inoue Y, Hoshino M, Takahashi H et al (2002) Bactericidal activity of Ag–zeolite mediated by reactive oxygen species under aerated conditions. J Inorg Biochem 92:37–42

Iravani S, Korbekandi H, Mirmohammadi SV, Zolfaghari B (2014) Synthesis of silver nanoparticles: chemical, physical and biological methods. Res Pharm Sci 9:385–406

Jana NR, Gearheart L, Murphy CJ (2001b) Wet chemical synthesis of high aspect ratio cylindrical gold nanorods. J Phys Chem B 105:4065–4067

Jana NR, Gearheart L, Murphy CJ (2001a) Wet chemical synthesis of silver nanorods and nanowires of controllable aspect ratio. Chem Commun 7:617–618

Jia T-J, Song GE, Li P-W et al (2008) Vibrational modes study of methyl orange using sers-measurement and the DFT method. Mod Phys Lett b, Condens Matter Phys, Stat Phys, Appl Phys 22:2869–2879

Jiang ZJ, Liu CY, Sun LW (2005) Catalytic properties of silver nanoparticles supported on silica spheres. J Phys Chem B 109:1730–1735. https://doi.org/10.1021/jp046032g

Jiang H, Moon K, Li Y, Wong CP (2006) Surface functionalized silver nanoparticles for ultrahigh conductive polymer composites. Chem Mater 18:2969–2973

Kabalnov A (2001) Ostwald ripening and related phenomena. J Dispers Sci Technol 22:1–12

Khan HI, Khan GA, Mehmood S et al (2019) Gold nanoworms: optical properties and simultaneous SERS and fluorescence enhancement. Spectrochim Acta Part A Mol Biomol Spectrosc 220:117111. https://doi.org/10.1016/j.saa.2019.05.016

Kruis FE, Fissan H, Rellinghaus B (2000) Sintering and evaporation characteristics of gas-phase synthesis of size-selected PbS nanoparticles. Mater Sci Eng b, Solid-State Mater Adv Technol 69:329–334

Li X, Shen J, Du A et al (2012) Facile synthesis of silver nanoparticles with high concentration via a CTAB-induced silver mirror reaction. Colloids Surfaces a, Physicochem Eng Asp 400:73–79

Li Y, Zhang W, Niu J, Chen Y (2013) Surface-coating-dependent dissolution, aggregation, and reactive oxygen species (ROS) generation of silver nanoparticles under different irradiation conditions. Environ Sci Technol 47:10293–10301

Liu X-H, Luo X-H, Lu S-X et al (2007) A novel cetyltrimethyl ammonium silver bromide complex and silver bromide nanoparticles obtained by the surfactant counterion. J Colloid Interface Sci 307:94–100

Liu H, Huang J, Gao Y et al (2013) Production of silver nanoparticles in a continuous stirred tank reactor based on plant-mediated biosynthesis: flow behaviors and residence time distribution prediction by computational fluid dynamics simulation. Ind Eng Chem Res 52:2280–2289

Liu J, Zhang C, Zhang S et al (2020) A versatile β-cyclodextrin functionalized silver nanoparticle monolayer for capture of methyl orange from complex wastewater. Chin Chem Lett 31:539–542

Mafuné F, Kohno J, Takeda Y et al (2000) Structure and stability of silver nanoparticles in aqueous solution produced by laser ablation. J Phys Chem B 104:8333–8337

Magnusson MH, Deppert K, Malm J-O et al (1999) Gold nanoparticles: production, reshaping, and thermal charging. J Nanoparticle Res Interdisc Forum Nanoscale Sci Technol 1:243–251

Mahapatra SS, Karak N (2008) Silver nanoparticle in hyperbranched polyamine: synthesis, characterization and antibacterial activity. Mater Chem Phys 112:1114–1119

Mayer M, Steiner AM, Röder F et al (2017) Aqueous gold overgrowth of silver nanoparticles: merging the plasmonic properties of silver with the functionality of gold. Angew Chemie (int Ed) 56:15866–15870

Medici S, Peana M, Nurchi VM, Zoroddu MA (2019) Medical uses of silver: history, myths, and scientific evidence. J Med Chem 62:5923–5943

Murphy CJ, Sau TK, Gole AM et al (2005) Anisotropic metal nanoparticles: synthesis, assembly, and optical applications. J Phys Chem B 109:13857–13870

Pathakoti K, Manubolu M, Hwang H-M (2017) Nanostructures: current uses and future applications in food science. Yàowu Shipin Fenxi 25:245–253

Pham TTH, Vu XH, Dien ND et al (2023) Synthesis of cuprous oxide/silver (Cu2O/Ag) hybrid as surface-enhanced Raman scattering probe for trace determination of methyl orange. R Soc Open Sci 10:221623

Saini R, Saini S, Sharma S (2010) Nanotechnology: the future medicine. J Cutan Aesthet Surg 3:32–33

Shu M, He F, Li Z et al (2020) Biosynthesis and antibacterial activity of silver nanoparticles using yeast extract as reducing and capping agents. Nanoscale Res Lett 15:14

Si MZ, Kang YP, Zhang ZG (2009) Surface-enhanced Raman scattering (SERS) spectra of methyl orange in Ag colloids prepared by electrolysis method. Appl Surf Sci 255:6007–6010

Slavin YN, Asnis J, Häfeli UO, Bach H (2017) Metal nanoparticles: understanding the mechanisms behind antibacterial activity. J Nanobiotechnol 15:65

Sohm B, Immel F, Bauda P, Pagnout C (2015) Insight into the primary mode of action of TiO_2 nanoparticles on *Escherichia coli* in the dark. Proteomics 15:98–113

Sondi I, Salopek-Sondi B (2004) Silver nanoparticles as antimicrobial agent: a case study on *E. coli* as a model for Gram-negative bacteria. J Colloid Interface Sci 275:177–182

Steinbrück A, Csaki A, Ritter K et al (2009) Gold and gold–silver core-shell nanoparticle constructs with defined size based on DNA hybridization. J Nanoparticle Res Interdiscip Forum Nanoscale Sci Technol 11:623–633

Sun Y, Yin Y, Mayers BT et al (2002) Uniform silver nanowires synthesis by reducing $AgNO_3$ with ethylene glycol in the presence of seeds and poly(vinyl pyrrolidone). Chem Mater 14:4736–4745

Tang S, Zheng J (2018) Antibacterial activity of silver nanoparticles: structural effects. Adv Healthc Mater 7:e1701503-n/a

Van Nguyen T, Vu DC, Pham VH et al (2021) Improvement of SERS for detection of ultra-low concentration of methyl orange by nanostructured silicon decorated with Ag nanoparticles. Optik 231:166431

Venditti I, Testa G, Sciubba F et al (2017) Hydrophilic metal nanoparticles functionalized by 2-diethylaminoethanethiol: a close look at the metal-ligand interaction and interface chemical structure. J Phys Chem C 121:8002–8013

Vorob'ev VV, Rogov AM, Osin YN et al (2018) Raman scattering of light by molecules of methyl orange dye on the surface of silicon containing ion-synthesized silver nanoparticles. Opt Spectrosc 124:649–654

Youssef AM, Abdel-Aziz MS, El-Sayed SM (2014) Chitosan nanocomposite films based on Ag-NP and Au-NP biosynthesis by *Bacillus subtilis* as packaging materials. Int J Biol Macromol 69:185–191

Yu C, Varghese L, Irudayaraj J (2007) Surface modification of cetyltrimethylammonium bromide-capped gold nanorods to make molecular probes. Langmuir 23:9114–9119

Zia R, Riaz M, Farooq N et al (2018) Antibacterial activity of Ag and Cu nanoparticles synthesized by chemical reduction method: a comparative analysis. Mater Res Express 5:75012